29th Congress of the International Council of the Aeronautical Sciences
St. Petersburg, Russia; September 7–12, 2014

INCOMPRESSIBLE TURBULENT FLOW AT THE LEADING OF SWEPT WINGS

E R Gowree*, C J Atkin*
***City University London**

Keywords: *swept wings, leading edge, turbulent boundary layer*

Abstract

Due to a singularity in the governing three-dimensional turbulent momentum integral equations at the attachment line, low order infinite-swept and swept-tapered CFD methods employing the viscous-coupling technique have been unable to model attachment line transition or contamination without approximating the development of the boundary layer immediately downstream of a turbulent attachment line. An experimental study was therefore conducted to explore the flow near a turbulent attachment line, which showed considerable differences to the numerical approximation. On the basis of the experimental data; a modification to the governing equations in the attachment line region has been proposed and tested. Comparisons with experimental measurements show that the proposed numerical model is not only able to predict the flow to within ±5%, but it also captures the non-monotonic behaviour of the momentum thickness, in the vicinity of the attachment line, which has not been reported previously.

1 Motivation

Much can be achieved in the conceptual stage of flow control research for transport aircraft wings by modelling the impact of such schemes on simple infinite-swept or swept-tapered configurations, which capture much of the three-dimensional flow physics in a two-degree-of-freedom problem. For aircraft wings operating at high Reynolds number, the flow along the attachment line of the wing is often turbulent and numerical methods, including low-order CFD codes, need to be able to predict the development of the wing boundary layer flow from a turbulent attachment line.

There is renewed interest in low-order CFD incorporating flow control modelling as a replacement for simple data-sheet methods for use in future project studies, for which traditional design rules are not reliable. CVGK is just such a low-order method, coupling the Airbus boundary layer code, Callisto, to the full potential method of Garabedian & Korn [1], extended to handle infinite-swept wing flows using Lock's transformation [2]. Callisto is a 2.5D turbulent boundary layer method based on the von Karman momentum integral equations, incorporating the lag-entrainment model of Green et al. [3], and modelling 3D turbulence using the streamline analogy. CVGK is the latest development of the viscous-inviscid-interaction (VII) method for transonic aerofoil flows originally developed at the Royal Aircraft Establishment [4]. The VII approach is described in detail by Lock & Williams [5], and has the advantage of requiring considerably less computing resource than RANS, with comparable accuracy for attached flows, while intrinsically delivering a breakdown of drag into friction, form and wave drag components. A recent numerical study conducted by Gowree [6] demonstrated that CVGK can predict the drag on swept wings in transonic flow with acceptable accuracy.

In the case of the turbulent attachment line (AL hereafter), the streamline analogy leads to singular governing equations in a very confined region downstream of the AL as a result of the streamline being locally perpendicular to the co-ordinate along which the boundary layer solver marches. At the AL itself the problem is resolved by invoking local

similarity arguments, but immediately downstream of the AL the singularity seemingly cannot be resolved. In CVGK this region is currently approximated by simply extrapolating the results of the AL calculation to about 0.5% of chord downstream.

The present work describes an experimental campaign which was launched (a) to validate the approximation and (b) to provide data for higher order CFD methods by mapping the turbulent flow in this relatively unexplored region, starting from the AL and progressing downstream to x/c = 0.03.

2 Numerical Modelling in Callisto

2.1 Numerical Approach

The numerical approach employed during the computational of a fully turbulent boundary layer along an infinite-swept wing using CVGK is presented in Atkin and Gowree [7]. In a simplified form the governing 3D momentum integral and entrainment equations, coupled with the transpiration velocity equation, can be expressed in a matrix system as

$$\begin{bmatrix} A_\theta & A_{\bar{H}} & A_\beta & A_U \\ E_\theta & E_{\bar{H}} & E_\beta & E_U \\ N_\theta & N_{\bar{H}} & N_\beta & N_U \\ W_\theta & W_{\bar{H}} & W_\beta & W_U \end{bmatrix} \frac{d}{d\xi} \begin{bmatrix} \theta \\ \bar{H} \\ \beta \\ U_e \end{bmatrix} = \begin{bmatrix} A_0 \\ E_0 \\ N_0 \\ W_0 \end{bmatrix} \quad (1)$$

The terms A and N denote the streamwise and normal momentum integral equations and E and W denote the entrainment and transpiration equations respectively. θ, $\bar{H}$, β, U_e and ξ are the momentum thickness, the incompressible shape factor, the angle between the external and limiting streamline, the velocity at the edge of the boundary layer and the streamwise coordinate respectively. For the full definition of these parameters, readers are referred to Atkin [8] or Gowree [6].

2.2 Leading Edge Approximation

The trajectory of the external inviscid streamline in vicinity of the AL is presented schematically in Fig. 1. At the AL the streamline angle $\psi_0 = \pi/2$ and, as the skin friction acts along the same axis as the AL, the angle between the limiting and the external streamline $\beta = 0$. Substituting these angles into the governing equations gives

$$\begin{aligned} A_\theta &= A_{\bar{H}} = A_\beta = A_U = 0 \\ E_\theta &= E_{\bar{H}} = E_\beta = E_U = 0 \\ N_\theta &= N_{\bar{H}} = N_\beta = N_U = 0 \\ W_\theta &= W_{\bar{H}} = W_\beta = W_U = 0 \end{aligned} \quad (2)$$

which leads to a singularity in the governing equations at the AL. Therefore in Callisto, Smith's formulation of the AL governing equations [9] is employed to initialise the boundary layer.

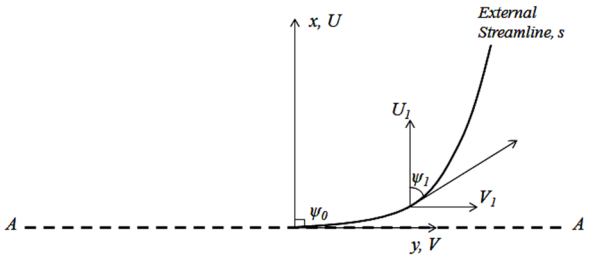

Fig. 1: The inviscid flow in the vicinity of the AL.

The singular behaviour persists downstream of the AL as ψ remains close to 90° and β very small, so the application of the full system of equations is delayed until $\psi_1 \leq 80°$. The turbulent AL solution for θ has to be imposed up to that position, sacrificing accuracy for numerical stability. Similar difficulties were encountered by Thompson and McDonald [10] and later by Smith [9] and a numerical approach similar to that in Callisto was adopted. Due to the small chordwise extent within which the approximation is applied (for most practical cases this region accounts for less than 1% of the chord length), it has been previously assumed that the prediction of the development of the boundary layer integral quantities downstream will not be affected, hence providing acceptable accuracy during the calculation of the profile drag.

However, recent studies into form drag reduction have raised concerns about this numerical fix, as the turbulent flow in the vicinity of the AL is very important for this type of analysis. Therefore further study is required either to validate the LE approximation or to propose a new approach to calculating the flow

immediately downstream of the AL where the numerical fix is currently applied.

3 Experiment

The experimental model used during the test was wooden, with a NACA0050 aerofoil profile, LE radius of curvature of *0.114m*, normal-to-LE chord length of *0.466m* and was swept by *60°*. It was mounted between the floor and ceiling of the test section of the T2 wind tunnel at the Handley Page Laboratory, City University London, as shown in Fig. 2. The T2 tunnel has a speed range of 4 to 55 m/s. A surface-mounted boundary layer traverse probe with micro-displacement capability was designed to capture the velocity profile, with a resolution of *2.5μm* per step achievable. Fig. 2 also shows the simple digital optical system used for near-wall alignment of the hot wire sensor and Fig. 3 shows three snap shots of the hot wire support in contact with the surface of the model at three different chordwise locations.

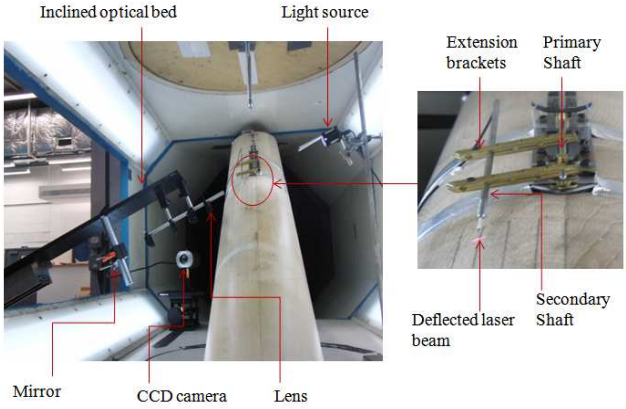

Fig. 2: Experimental set-up and hot-wire alignment.

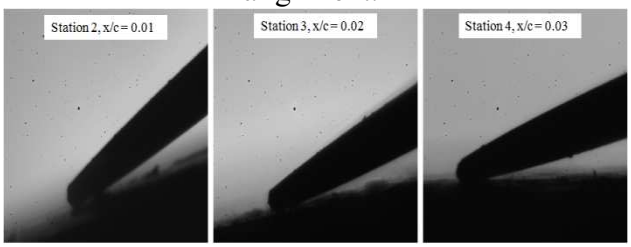

Fig. 3: Snapshot of the side of the hot wire support in contact with the surface.

A single normal (SN) hot wire probe, Dantec 55P15, was used to capture the single velocity component at the AL and a single yawed (SY) probe, Dantec 55P12, for the measurement of the two in-plane velocity components downstream of the AL. The constant temperature anemometry (CTA) technique was used and the hot wire probes were connected to the DISA-55M10 CTA Standard Bridge (M-Unit) module, which consists of a Wheatstone bridge equipped with a servo mechanism. The M-Unit was in turn interfaced with a National Instruments (NI)-DAQ card with built-in A/D converter and installed in a PC for data acquisition using NI-Labview. The hot wire output signal was pre-filtered through a low-pass filter rated at 4.8 kHz prior to recording. King's law was applied for the reduction of hot wire output voltage. The calibration of the SN probe and measurement of a single velocity component at the AL was straight forward, but more challenging for the SY probe for the two velocity components measurement downstream. In this case Bradshaw's method was employed and a yaw calibration was required due to the directional sensitivity of the SY probe.

Preston's technique was employed for the measurement of local surface shear stress. At the AL, the flow resolves into a single, spanwise velocity component, similar to the streamwise flow along a flat plate, thus the method should yield reasonable accuracy. This technique has been restricted to 2D flows where the skin friction is acting along the same axis as the velocity component; therefore for the flow downstream of the AL an attempt was made to extend this technique to the 3D boundary layer under the highly curved streamline at the LE of a swept wing. The surface shear stress measurement was made by aligning the Pitot-tube in the direction of the local external streamline, obtained from the velocity components at the edge of the boundary layer.

4 Experimental Results

4.1 Turbulent Attachment Line

The velocity profile was initially captured at the AL and good agreement was observed between the laminar velocity profile measurements and theory (swept Hiemenz flow) for lower Reynolds number. However, due to contamination by the turbulent boundary layer on the floor of the wind tunnel, the AL was turbulent for $R_\theta > 100$. This threshold is in

agreement with the results of Pfenninger [11] and Gaster [12]. The turbulent mean velocity profiles were captured at various AL Reynolds numbers and, using the surface shear stress measurements these profiles were represented in wall units, Fig. 4. For the fully turbulent velocity profiles, some measurements were achieved in the laminar sub-layer despite a boundary layer thickness of the order of *3mm*, owing to the digital optical system which enabled alignment of the hot wire probe very close to the wall. Fig. 4 shows that the logarithmic region of the velocity profiles deviates from the universal log-law used by Cumpsty and Head [13], although significant scatter can be seen in the latter's experimental results. In the present work the log-law was modified according to the DNS analysis of Spalart [14] who suggested that, for $R_\theta < 600$, the log-law was defined by the von Karman constant, $k < 0.41$.

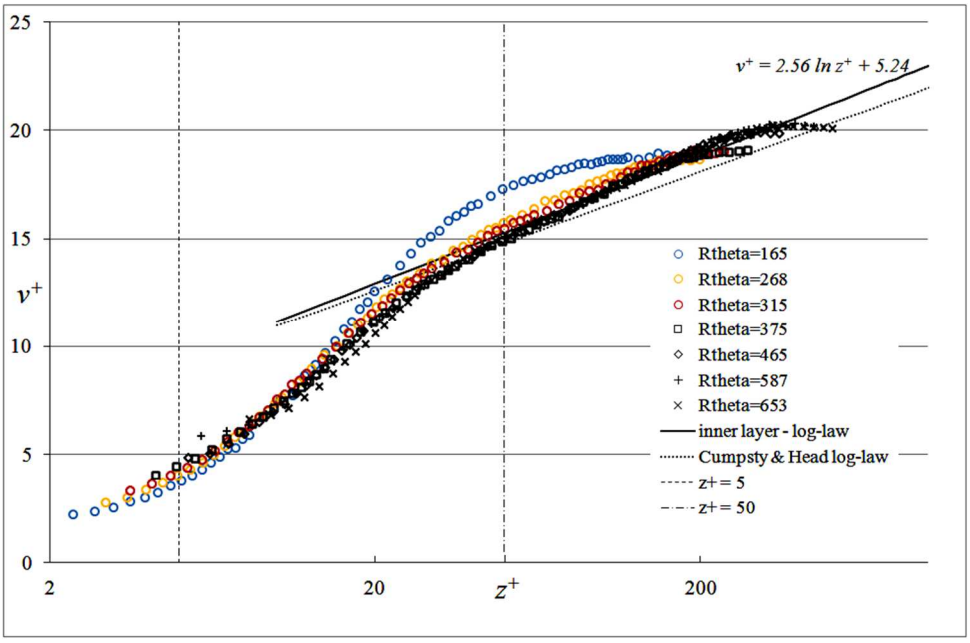

Fig. 4: The turbulent velocity profile at the AL.

4.2 Turbulent Flow Downstream of the Attachment Line

The measurement of the turbulent boundary layer downstream of the AL was more challenging due to the presence of both streamwise and crossflow velocity components. A 2-component single yawed (SY) hot wire was employed in preference to a cross-wire due to the thinness of the boundary layer. A novel approach was adopted to determine the velocity components from the hot-wire signals: the measurements where made with the hot-wire mounted first in a clockwise and then in an anticlockwise orientation with respect to the mean-flow, which meant that the same traverse profile had to be repeated for all measurement stations.

4.2.1 Streamwise Velocity Profiles

The mean streamwise velocity profiles captured downstream of the AL on both the port and starboard side of the model are presented in Fig. 5, for an AL Reynolds number $R_\theta = 590$. The good agreement between the port and starboard side measurements confirms that the AL was located at *x/c = 0* and therefore that the model was symmetrical and at zero incidence.

Using the surface shear stress measurements the velocity profiles were represented in wall units as shown in Fig. 6. The inner region of the velocity profiles matched the 'universal log-law' with reasonable agreement, but the measurements in the viscous sub-layer does not show any trend with chordwise position. At x/c = 0.02, for $y^+ \approx 10$,

the first couple of data points are more or less the same, unlike the profiles at the remaining chordwise locations and this might be due to the inability of capturing the flow very accurately near the wall due to surface curvature. However, the agreement with the universal log-law, Fig. 6, suggests that the profiles were captured with reasonable accuracy and be used for further analysis.

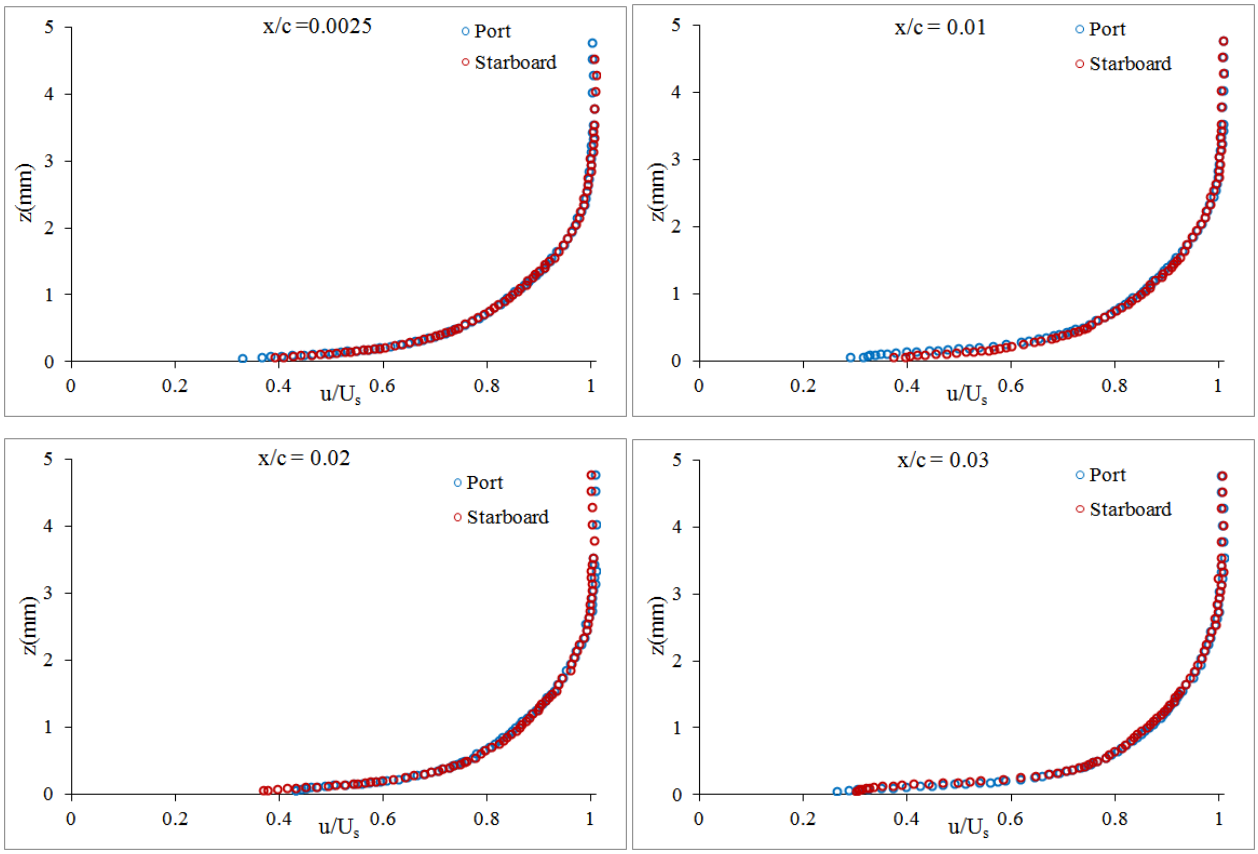

Fig. 5: Streamwise velocity profiles downstream of the AL at $R_\theta = 590$.

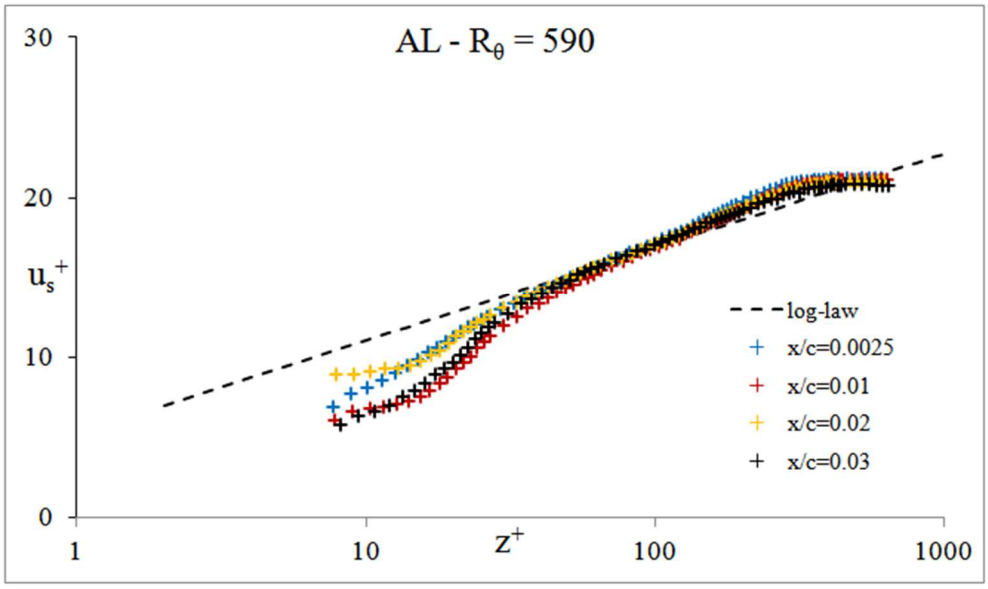

Fig. 6: Streamwise velocity profiles in wall units downstream of the AL at $R_\theta = 590$.

4.2.2 Crossflow Velocity Profiles

Fig. 7 shows the crossflow velocity profiles at different chordwise positions downstream of the AL. Good agreement can be observed between the port and starboard measurements except at *x/c = 0.03*. This was due to the limitation in the yaw sensitivity of the SY probe which was therefore restricted to ±70˚ during the yaw calibration. More details of the crossflow were revealed when the profiles were plotted on the triangular hodograph model proposed by Johnston [15], as shown in Fig. 8, where the crossflow is normalised by streamwise velocity. From Fig. 8 it is easier to identify the point where the crossflow changes direction and where 'S-type' or 'cross-over' crossflow profiles first appear, at x/c > 0.0025. Normally the cross-over point occurs very close to the wall and shifts upwards further downstream, as observed in Fig. 8. Due to the difficulties in near wall measurement it is difficult to capture the chordwise location where the cross-over is incipient. The main issue with the triangular representation is the difficulty in applying a linear fit to the profiles especially near the peak values of the crossflow velocity.

According to Johnston the angle between the limiting and the external streamline, β, can be approximated as the gradient of the line of best fit connecting the origin and the apex of the triangle formed by the stationary points (maxima or minima) of the velocity profiles, assumed to be the region where the surface shear stress is dominant.

Using this approach, on the port side of the model, at *x/c = 0.0025*, the angle between the limiting and external streamline, $\beta = -4.9°$. The same method applies to the cross-over profile, but due to insufficient data in the near wall region for $0.01 \leq x/c \leq 0.02$, it was not possible to determine β until *x/c = 0.03,* where the apex of the triangle could be resolved. At this position the angle was calculated as $\beta = 5.9°$. From Fig. 8 the cross-over in the crossflow profiles starts immediately downstream of *x/c=0.0025*, so that β does not increase to large negative values but actually changes sign. Therefore, it is fair to assume that, within the experimental domain, the limiting streamline angle ranged between $-5° < \beta < 6°$.

4.2.3 The Boundary Layer Integral Quantities

The streamwise and crossflow boundary layer integral quantities in an incompressible 3D boundary layer can be defined as

$$\delta_1^* = \int_0^\delta \left(1 - \frac{u}{U_s}\right) dz, \qquad \delta_2^* = -\int_0^\delta \frac{v}{U_s} dz$$

$$\theta_{11} = \int_0^\delta \frac{u}{U_s}\left(1 - \frac{u}{U_s}\right) dz, \qquad \theta_{21} = \int_0^\delta \frac{uv}{U_s^2} dz$$

$$\theta_{12} = \int_0^\delta \frac{v}{U_s}\left(1 - \frac{u}{U_s}\right) dz, \qquad \theta_{22} = \int_0^\delta \frac{u^2}{U_s^2} dz$$

where u and v are the local velocity components parallel and normal to the streamline velocity U_s at the boundary layer edge. The development of these integral quantities near the AL, determined from the experimental u and v profiles, is presented in Fig. 9. The streamwise momentum thickness, θ_{11}, increases by approximately 15% immediately downstream of the AL as does the streamwise displacement thickness, δ_1^*. Slight non-monotonic behaviour can be observed in the development of θ_{11} and δ_1^*, but this effect might also be due to experimental error. The crossflow momentum thicknesses, θ_{12} and θ_{22}, are almost negligible at the AL (equal to zero in theory) and do not vary significantly downstream, but θ_{21} and δ_2^* attain a value of approximately 35% of the streamwise displacement and momentum thickness. This increment in the integral quantities is significant but is not captured by Callisto due to the singular nature of the governing equations in this region.

5 Modification to Leading Edge Modelling

In Callisto the LE approximation is applied for $\psi_1 \leq 80°$ and, from the streamwise velocity at the edge of the boundary layer, this region lies within $0.005 < x/c < 0.01$, where the limiting streamline angle can be approximated as $-4° < \beta < 4°$. Therefore, in the proximity of the AL $\tan\beta \approx 0$, as β is small, but $\partial\beta/\partial x \neq 0$. Based on this assumption the normal momentum integral equation can be modified and a new set of governing equations are derived applicable to the region previously approximated in Callisto.

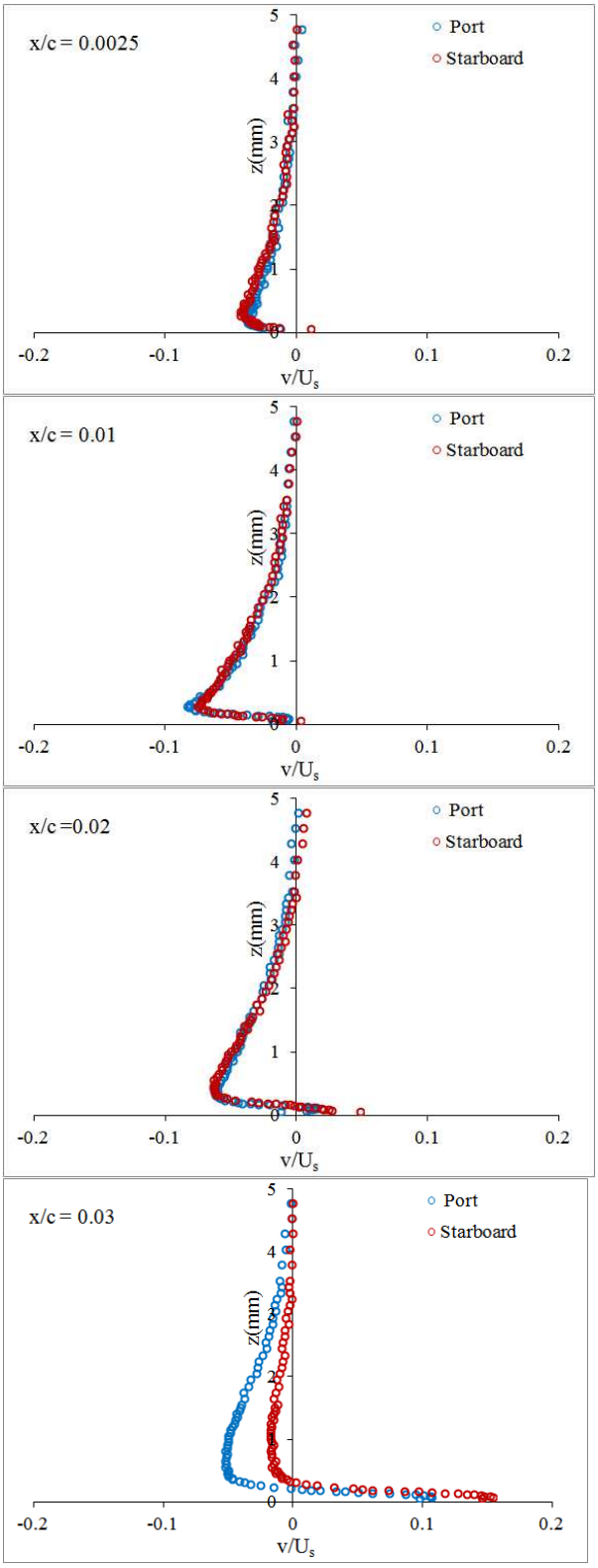

Fig. 7: Crossflow velocity profiles downstream of the AL at $R_\theta = 590$.

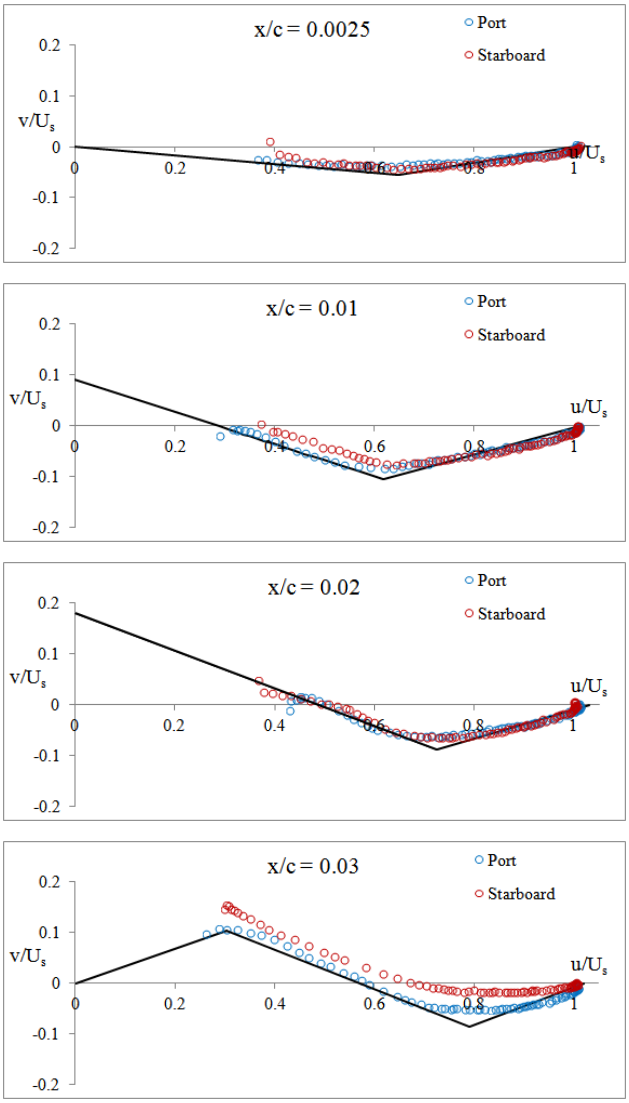

Fig. 8: Triangular representation of crossflow profiles using Johnston's model.

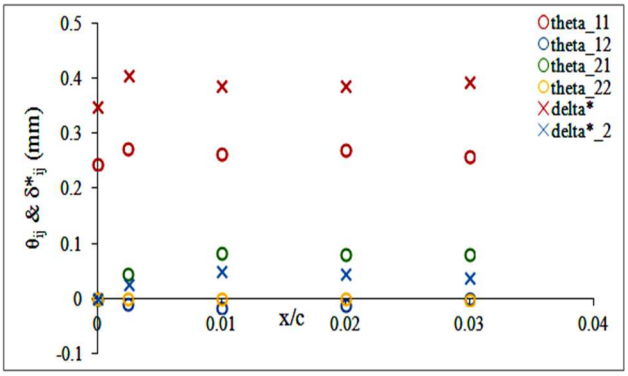

Fig. 9: The port side streamwise and crossflow integral quantities (defined in section 4.2.3) near the AL at $R_\theta = 590$.

More details of the derivation of the governing equations are available in reference [6]. The improved LE modelling allows the computation of the turbulent 3D boundary layer over the full chord of an infinite swept wing. The development of the streamwise momentum thickness obtained from the computation with the improved LE modelling (new) can be compared with those from the previous version of Callisto (old) in Fig. 10, where s/c represents the normalised coordinate along the surface of wing profile. The computation with the modified version was conducted for both the geometrical sweep angle, 60°, and the effective sweep which was calculated to be approximately 62° using the experimental static pressure at *x/c=0*.

Fig. 10 illustrates how the previous version of Callisto, fixes θ at a constant value immediately downstream of the AL; θ starts to increase again once a solution of the full governing equations is obtained for $\psi_1 > 80°$. In the modified version, the full governing equations can be solved immediately downstream of the AL: Fig. 10 shows a significant improvement in the predicted development of θ, as the momentum thickness is predicted to be within ±5% of that obtained experimentally. More importantly, the non-monotonic behaviour in the experimental θ is replicated by the numerical results, hence supporting the initial experimental observation.

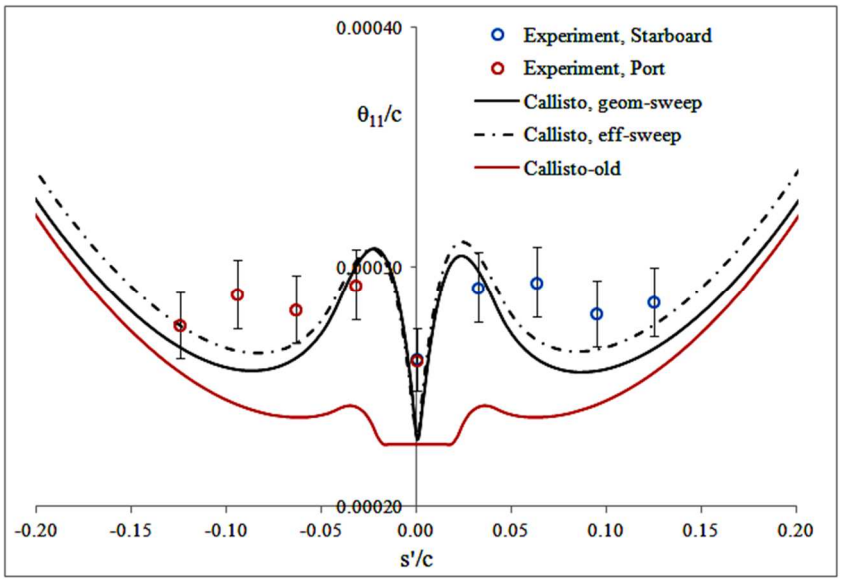

Fig. 10: Comparison of θ captured experimentally against those computed using the previous and the modified version of Callisto.

6 Discussion

Fig. 4 also shows that, for $R_\theta \geq 315$, the linear region of the velocity profiles collapse onto the modified log-law. This finding is in agreement with Preston's criterion for the minimum Reynolds number for the existence of a fully turbulent boundary layer on a flat plate, $R_\theta \approx 320$. Based on this result a new regime where the AL is intermittent can be defined for $100 < R_\theta < 315$. Unfortunately the AL has been previously misinterpreted to be fully turbulent in this regime, which is misleading. In addition, on the mid-span and outboard wing of short-haul, and the outboard wing of long-haul transonic aircraft, $R_\theta < 300$: therefore numerical analysis assuming fully turbulent flow right from the AL is potentially inaccurate.

The considerable increase in the boundary layer integral quantities immediately downstream of the AL supports the need for a model to capture these behaviours not previously represented in Callisto. The modified set of near-attachment governing equations, derived on the basis of the experimentally-observed behaviour of β, are both numerically

robust and more faithful to the experimental development of momentum thickness near the AL. Despite the significant improvement in the leading edge modelling using the proposed modification, profile drag predictions were not significantly affected as the predicted momentum thickness in the far wake was very similar for both the old and the new version of Callisto. Due to the presence of the favourable pressure gradient at the leading edge, the growth in momentum thickness is very slow and, at x/c>0.25, the θ predictions from the two methods converge, as indicated by the numerical results in Fig. 10. Moreover, in the vicinity of the AL, θ is small compared to its magnitude in the far wake which determines the profile drag coefficient of the wing section.

From the mean flow measurements it is difficult to understand and describe the physical mechanism responsible for the non-monotonic growth in θ in the vicinity of the AL, but as a similar trend was predicted by Callisto a simple diagnosis was conducted by analysing the individual terms of the streamwise momentum integral equation. The stationary points in the trend of θ appear when the magnitude of the favourable pressure gradient, initially perpendicular to the streamline, eventually overtakes the skin friction immediately downstream of the AL, hence slowing the growth in θ, which results in a maximum. The minimum is associated with the point where skin friction, perhaps responding to the thinning of the boundary layer, exceeds the magnitude of the favourable pressure gradient, so that θ grows again. Similar behaviour was also observed in the calculation of the flow over a transonic wing at cruise condition.

The current experimental results can help in the validation of higher-order turbulence models which aim to capture the effect of lateral straining from highly diverging or converging streamlines.

7 Conclusions

Experimental measurements near the AL have led to the proposal of a minimum Reynolds number for a turbulent AL which is in agreement with Preston's criterion for the flow on a flat plate.

Based on the observed small magnitude of the limiting streamline angle, β, a new simplification to the turbulent boundary layer equations has been derived for the AL region. The results from the new model show good agreement with the experimental results, in particular reproducing the non-monotonic behaviour in θ.

Further Reynolds stress measurements will be required to understand the physical mechanism responsible for such behaviour in the vicinity of the AL.

Acknowledgement

This study was supported by EADS Innovation Works (now Airbus Group Innovations) under studentship agreement IW10430.

References

[1] Garabedian P R and Korn D G. Analysis of transonic aerofoil. Communications on Pure and Applied Mathematics. Vol. 24, 1971.

[2] Lock R C. An equivalence law relating three- and two-dimensional pressure distributions. NPL Aero Report no. 1028, 1962.

[3] Green J E, Weeks D J and Brooman J W F. Prediction of turbulent boundary layers and wakes in compressible flow by lag-entrainment method. ARC R&M 3791, 1973.

[4] Ashill P R, Wood R F and Weeks D J. An improved, semi-inverse method of the viscous Garabedian and Korn method (VGK). RAE TR 87002, 1987.

[5] Lock R C and Williams B R. Viscous and inviscid interactions in external aerodynamics. Progress in Aerospace Science, Vol. 24, 1987.

[6] Gowree E R. Influence of Attachment Line on Form Drag. PhD Thesis, City University London, 2014

[7] Atkin C J and Gowree E R. Recent Development to the Viscous Garabedian and Korn Method. 28th ICAS, Brisbane, 2012.

[8] Atkin C J. Summary of the Swept-Tapered Lag-Entrainment Boundary Layer Method in Callisto version 3.4. Technical Report QinetiQ/08/00064, 2008.

[9] Smith P D. A calculation method for the turbulent Boundary layer on an infinite yawed wing in compressible , adiabatic flow. ARC CP 1268, 1974.

[10] Thompson B G J and McDonald G J. The prediction of boundary layer behaviour and profile drag for infinite swept wings: Part III a method for calculation. ARC CP 1309, 1973.

[11] Pfenninger W. Flow Phenomena at the Leading Edge of Swept wings, Recent development in Boundary Layer Research. AGARDograph 97, 1965.

[12] Gaster M. On the flow along swept leading edges. Aeronautical Quarterly, Vol. 17, 1967.

[13] Cumpsty N A and Head M R. The Calculation of the Three-Dimensional Turbulent Boundary Layer. Part III: Comparison of the Attachment Line Calculations with Experiment. Aeronautical Quarterly, Vol. 20, 1969.

[14] Spalart P R. Direct Simulation of a Turulent Boundary layer up to R=1410. J. Fluid Mech., Vol. 187, 1988.

[15] Johnston J P. On the three dimensional boundary layer generated by secondary flows. Journal of Basic Engineering, Series D, Trans. ASME, Vol. 82, 1960.

Contact Author Email Address

erwin.gowree.1@city.ac.uk

Copyright Statement